AGU PUBLICATIONS

JGR

Journal of Geophysical Research: Space Physics

RESEARCH ARTICLE
10.1002/2016JA022635

Key Points:
- Intermediate scale (100 m to few kilometers) ESF irregularities at unusually higher altitude
- Large-scale structures with stronger ΔN near raised equatorial F peak
- A large deviation of 230 m/s in low-latitude F region zonal irregularity drift

Correspondence to:
B. Kakad,
bkakad9@gmail.com

Citation:
Kakad, B., P. Gurram, P. N. B.Tripura Sundari, and A. Bhattacharyya (2016), Structuring of intermediate scale equatorial spread *F* irregularities during intense geomagnetic storm of solar cycle 24, *J. Geophys. Res. Scape Physics*, *121*, doi:10.1002/2016JA022635.

Received 21 AUG 2015
Accepted 5 JUL 2016
Accepted article online 11 JUL 2016

Structuring of intermediate scale equatorial spread *F* irregularities during intense geomagnetic storm of solar cycle 24

B. Kakad[1], P. Gurram[1], P. N. B. Tripura Sundari[2], and A. Bhattacharyya[1]

[1]Indian Institute of Geomagnetism, Panvel, India, [2]Space Physics Laboratories, Department of Physics, Andhra University, Visakhapatnam, India

Abstract Here we examine the structuring of equatorial plasma bubble (EPB) during intense geomagnetic storm of solar cycle (SC) 24 that occurred on 17 March 2015 using spaced receiver scintillation observations on a 251 MHz radio signal, recorded by a network of stations in Indian region. As yet, this is the strongest geomagnetic storm ($Dst_{min} \sim -223$nT) that occurred in present SC. Present study reveals that the structuring of equatorial spread *F* (ESF) irregularities was significantly different on 17 March as compared to quiet days of corresponding month. ESF irregularities of intermediate scale (100 m to few kilometers) are observed at unusually higher altitudes ($\geq$ 800 km) covering wider longitudinal-latitudinal belt over Indian region. A presence of large-scale irregularity structures with stronger ΔN at raised *F* peak with small-scale irregularities at even higher altitudes is observed. It caused strong focusing effect ($S_4 > 1$) that prevails throughout premidnight hours at dip equatorial station Tirunelveli. Other observational aspect is that zonal irregularity drifts over low-latitude station Kolhapur exhibited a large deviation of ~230 m/s from their average quiet time pattern. During this geomagnetic storm, two southward turnings of significant strength ($B_Z \leq -15$ nT) occurred at 11.4 IST (Indian standard time) and 17.9 IST. The later southward turning of interplanetary magnetic field (IMF) B_Z resulted in a large eastward prompt penetration electric field (PPEF) close to sunset hours in Indian longitude. Estimates of PPEF obtained from real-time ionospheric model are too low to explain the observed large upliftment of *F* region in the post sunset hours. Possible reason for observed enhanced PPEF-linked effects is discussed.

1. Introduction

Often, a spectacular phenomenon is observed in the equatorial *F* region during post sunset hours, known as equatorial spread *F* (ESF). Particularly, day-to-day occurrence of ESF, through nonlinear evolution of Rayleigh-Taylor (RT) plasma instability, is of great interest as these irregularities cause degradation of incoming radio signal. It is widely known that the occurrence of equatorial plasma bubbles (EPBs) varies with solar flux, seasons, geomagnetic activity, longitude, and latitude [*Burke et al.*, 2004; *Nishioka et al.*, 2008]. Generation of EPBs resulting from geomagnetic disturbance is known for past few decades. During periods of geomagnetic storm, disturbance dynamo (DD) and prompt penetration (PP) of magnetospheric electric field are the two major sources for modulation of ambient ionospheric electric field [*Blanc and Richmond*, 1980; *Spiro et al.*, 1988; *Fejer et al.*, 1990]. The effects observed at ionospheric *F* region are associated with DD or PP or a combination of both DD and PP electric fields [*Maruyama et al.*, 2005; *Kakad et al.*, 2007, 2011, 2012a]. Westward to eastward turning of the ambient electric field that results from superimposed disturbed time electric fields (DD/PP/DD+PP) raises the equatorial *F* region to higher altitudes, where RT plasma instability can be initiated with appropriate seeding perturbation to give rise to EPBs. *Li et al.* [2010] showed that the combined effects of prompt penetration electric field (PPEF) and disturbance dynamo electric field (DDEF) can result in a wide longitude extent of ionospheric irregularities.

Each geomagnetic storm is different from the other as the characteristics of their driving source are not same. Also, their start time, strength, and interplanetary characteristics differ from one geomagnetic storm to the other. Depending on strength and direction of equatorial ionospheric electric fields at a particular longitude resulted from this magnetic activity, the EPBs can be either generated or inhibited at equatorial *F* region at those longitudes [*Sastri*, 1999; *Abdu et al.*, 1997; *Martinis et al.*, 2005]. The prediction of geomagnetic activity-linked EPBs is crucial, and it is of global interest. However, more than just the occurrence of EPBs,

their spatial evolution is of greater interest because the structuring of ESF irregularities can be significantly different during geomagnetically active periods [*Keskinen et al.*, 2006], and it can cause severe degradation to incoming radio signals. Spaced receiver scintillation technique is a useful tool to investigate spatial scale lengths of ESF irregularities using method introduced by *Bhattacharyya et al.* [2003]. This technique is applicable to both weak and strong scintillations unlike power spectral analysis technique, which is valid for only weak scintillations. Recently, *Yadav et al.* [2015] examined the spatial structures of *E* region long-wavelength irregularities using daytime spaced receiver VHF scintillation observations. Besides this it can be used to get the zonal irregularity drift.

Recently intense geomagnetic storm occurred on 17 March 2015, which happens to be the strongest magnetic storm so far in the present solar cycle (SC). We have examined the effect of this geomagnetic storm on low-latitude *F* region over Indian longitude with particular focus on structuring and evolution of EPBs developed due to electric fields associated with this magnetic activity. It is found that on 17 March, *F* region uplifted to unusually higher altitudes, where EPBs are triggered, and evolved nonlinearly to produce ESF irregularity structures having wider longitudinal and latitudinal coverage in the Indian region in the post sunset hours. Structuring of the generated EPBs is found to be considerably different on 17–18 March as compared to that on quiet days of March 2015. Spaced receiver VHF scintillation observations from network of Indian low-latitude stations are used in the present study. The details of data and analysis technique are given in section 2. Results are discussed in section 3. Characteristics of geomagnetic storm and ionospheric model outputs are presented in section 4. The present work is summarized and concluded in section 5.

2. VHF Scintillation Observations and Data Analysis Technique

Here we use amplitude scintillations on 251 MHz signal transmitted from geostationary satellite UFO10 (72.4°E) and recorded by network of spaced receivers at low-latitude stations during March 2015. These spaced receivers are closely aligned along magnetic east-west at stations Tirunelveli (TIR, 8.7°N, 77.8°E, dip latitude 1.5°N), Kolhapur (KOP, 16.68°N, 74.26°E, dip latitude 10.4°N), and Allahabad (ALD, 25.2°N, 81.5°E, dip latitude 21.8°N). Single receiver amplitude scintillations on the same frequency recorded at Mumbai (MUM, 19.09°N, 72.85°E, dip latitude 14.5°N) are also utilized. The zenith θ and azimuth A angle of the signal path transmitted from UFO10 at above mentioned stations are TIR 12.8° and 216.9°, KOP 19.89° and 190.2°, and ALD 31.7° and 202.8°, respectively. The distance between two receivers x_0 at these stations is 540 m, 265 m, and 484 m, respectively. Amplitude scintillations are sampled at every 0.05 s.

Location of observation stations on India's map is shown in Figure 1a. It is important to note that these stations do not lie in the same magnetic longitude. The location of these stations is such that TIR (geomagnetic longitude 150.4°E), KOP (geomagnetic longitude 147.7°E), MUM (geomagnetic longitude 146.6°E), and ALD (geomagnetic longitude 155.4°E) nearly cover a longitudinal (latitudinal) area of $\approx$ 8.8° (16.6°). It corresponds to a distance of 1030 km (1940 km) at a height of 300 km. ESF irregularities are highly magnetic field aligned. Earth's magnetic field lines can be represented by $r/R_E = L\cos^2(\Psi)$, where L is the distance from the center of the Earth of the equatorial crossing point of the magnetic field line in units of Earth's radius (R_E) and Ψ is the magnetic latitude. The path followed by magnetic field lines at different altitudes is displayed in Figure 1b, and it indicates that the ESF irregularities situated at an altitude of ~800 km close to magnetic equator can map down to low midlatitude station ALD at ~ 250 km through highly conducting magnetic field lines. This limiting apex height is shown by horizontal red dotted line in Figure 1b.

Recorded spaced receiver scintillation observations are analyzed using full cross-correlation technique [*Briggs*, 1984], and parameters S_4, V_0, V_C, and $C_l(x_0, t_m)$ are computed for every 3 min [*Engavale et al.*, 2005]. S_4 is a measure of strength of scintillations. Random velocity V_C provides the measure of random changes in the irregularity characteristics. V_0 is the average drift of the ground scintillation pattern in the receivers plane, which is determined by the drift of the irregularities across signal path. $C_l(x_0, t_m)$ is the maximum cross correlation between intensity variations recorded by two receivers during each interval of 3 min. V_0 and V_C are estimated only if $C_l(x_0, t_m) \geq 0.5$; as in this regime assumed form of space time correlation function of intensity variations in the full correlation analysis has greater validity. It should be noted that incoming radio signal has nonzero zenith and azimuth angle. Thus, V_0 provides the average of projection of irregularity drift transverse to signal path in receivers plane. Considering the geometry of the incoming radio signal, we get $V_0 = V_X - V_Z \tan\theta \sin A$, where V_X and V_Z are eastward and vertical drift of irregularities. Substitution of zenith and azimuth of a signal path in above expression indicates that an amount of $-0.13V_Z$, $-0.06V_Z$, and $-0.24V_Z$

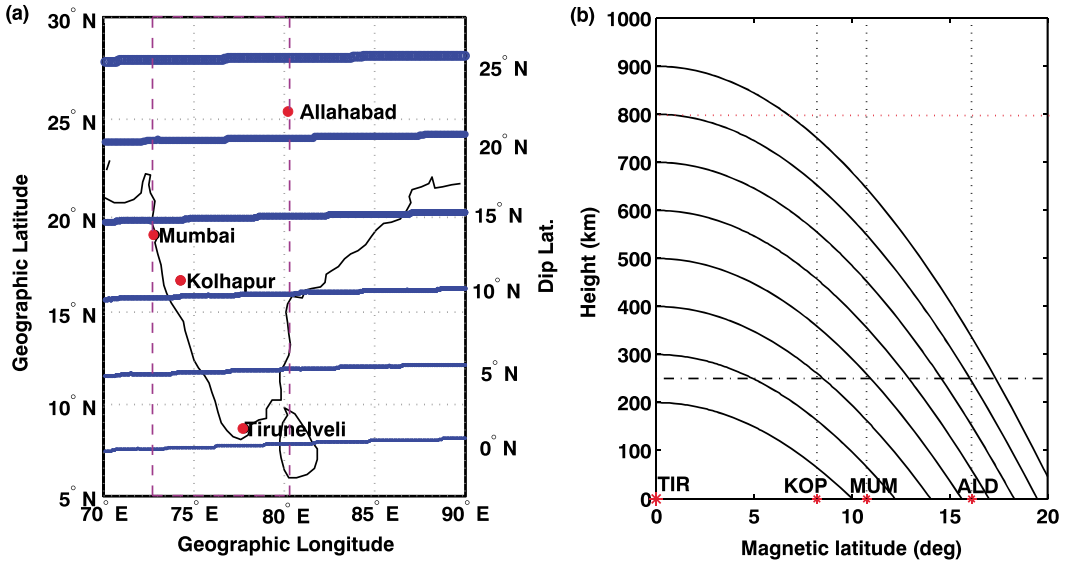

Figure 1. (a) Location of observation stations is marked on India's map. These stations longitudinally and latitudinally cover nearly 8.8° and 16.5°, respectively. Horizontal blue lines represent dip latitude. (b) The path followed by geomagnetic field lines as a function of altitude and geomagnetic latitude. Magnetic field line situated at 800 km (horizontal red dotted line) at magnetic equator can map down to an altitude of 250 km (horizontal black dotted line) at low midlatitude station Allahabad.

contributes to V_0 at TIR, KOP, and ALD, respectively. On 17–18 March, only single receiver scintillation observations were available from TIR and ALD. Hence, we could estimate V_0, $C_l(x_0, t_m)$, and V_C only for KOP station. For 17–18 March scintillation observations from KOP are analyzed for every 1.5 min.

3. Results and Discussion

Here we have examined the effect of geomagnetic storm of 17 March 2015 on (i) *F* region zonal plasma drifts and (ii) structuring of ESF irregularities in post sunset hours. The occurrence/nonoccurrence (suppression) of EPBs is related to the upward/downward movement of *F* region in the post sunset hours resulting from superimposed disturbed time eastward/westward electric field. In the presence of favorable ambient conditions, EPBs can be generated through RT instability only with an appropriate seeding perturbation. On the other hand former effect mentioned above is related to disturbed time changes in equatorial electric field due to modified neutral wind caused by magnetic activity. Although both effects are linked with magnetic activity, they are driven by different physical processes, which are discussed in the following sections.

3.1. Effect on Zonal Drifts

Parameters retrieved from spaced receiver scintillations, namely, S_4, V_0, V_C, and $C_l(x_0, t_m)$, on 17–18 March (red) and corresponding quiet days (black) are shown as a function of Indian standard time (IST) in Figure 2 for off equatorial station KOP. As seen in Figure 2, V_0, V_C, and $C_l(x_0, t_m)$ follow a well-defined pattern for magnetically quiet days. In the initial phase of development of EPB the signals from two receivers are highly decorrelated giving rise to lower values of $C_l(x_0, t_m)$. Also, the random velocity, V_C, is higher indicating the rapid changes in the characteristics of generated ESF irregularities. When the perturbation electric field associated with RT plasma instability is considerably eroded, $C_l(x_0, t_m)$ tends to approach higher correlation with lower values of V_C [*Bhattacharyya et al.*, 1989, 2001; *Engavale et al.*, 2005]. Figure 3a shows monthly quiet time average irregularity drifts, $\langle V_0 \rangle_Q$, along with disturbed time irregularity drift, V_D, seen at KOP. These averages are estimated for every 10 min interval. To obtain a quantitative estimate of the effect of geomagnetic activity on V_0, we removed the quiet time average from that on geomagnetically disturbed day (i.e., $\Delta V = V_D - \langle V_0 \rangle_Q$), and it is plotted as a function of IST in Figure 3b. A large deviation of magnitude 227 m/s at around 22.33 IST is observed in the irregularity drifts at KOP, which is indicated by vertical dash-dotted line in Figure 3b.

The evident observational features of Figures 2 and 3 are as follows. (i) Scintillations are initiated earlier on 17 March, and they are stronger in the initial phase as compared to quiet days of that month; (ii) irregularity drift, V_0, decreases rapidly and turns westward; (iii) random velocity shows large values (≈ 100 m/s) indicating

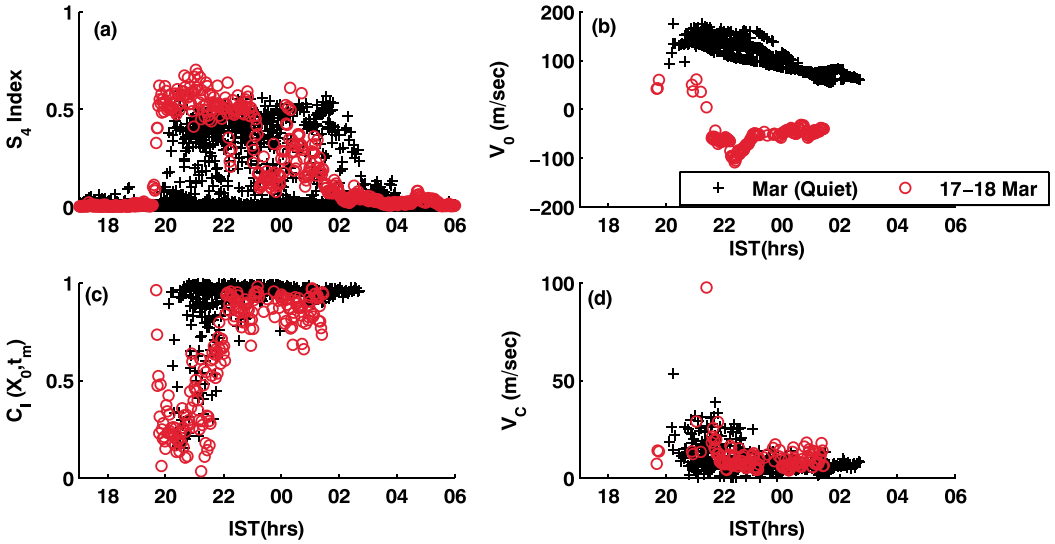

Figure 2. Quiet (black) and disturbed time variation, 17–18 March (red), of (a) S_4 Index, (b) V_0, (c) $C_I(x_0, t_m)$, and (d) V_C for off equatorial station Kolhapur.

highly evolving perturbation electric fields that are linked with RT instability; and (iv) $C_I(x_0, t_m)$ shows low values for a longer duration as compared to their quiet time pattern. Earlier studies have demonstrated that westward drifts are superimposed on ambient zonal plasma drifts on geomagnetically disturbed days [*Fejer et al.*, 1991; *Fejer and Scherliess*, 1995; *Scherlies and Fejer*, 1997; *Sutton et al.*, 2005; *Ma and Maruyama*, 2006]. It results in considerable decrease in the eastward zonal plasma drifts or sometimes their east to westward reversal. These magnetic storm time westward zonal drifts are attributed to enhanced heating of neutrals at high latitudes due to increased conductivities and currents (Joule heating). The process is known as DD, which is set up by neutral wind propagation from high to low latitudes. During its propagation the neutral wind experiences westward deflection due to Coriolis force in the middle to low latitudes [*Abdu*, 2012], finally resulting in a westward plasma drift at low latitudes.

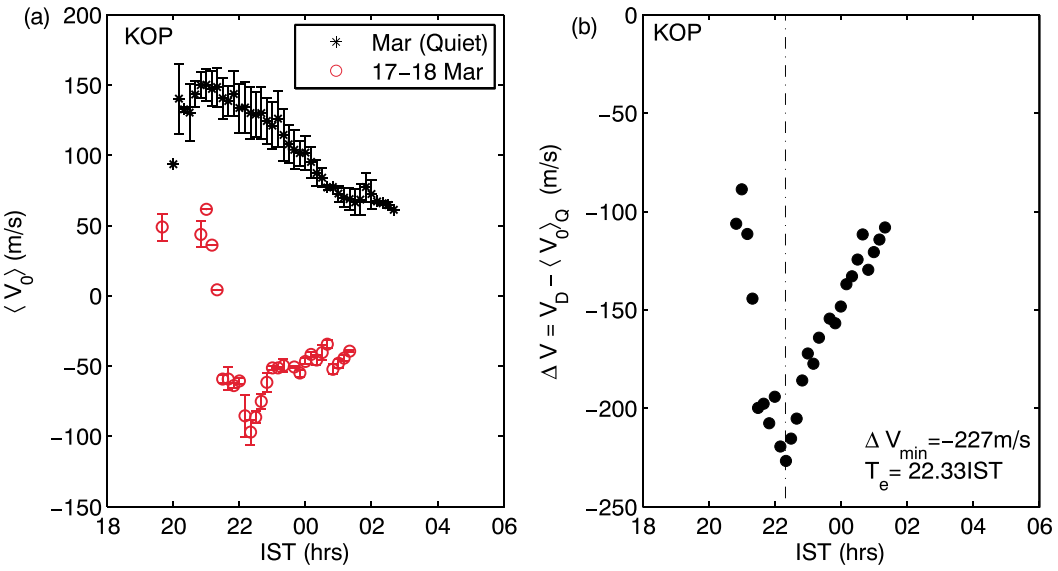

Figure 3. Variation of (a) monthly quiet time average of V_0 along with disturbed time (17–18 March) V_0 and (b) deviation in V_0 on disturbed day 17–18 March, represented by $\Delta V = V_D - \langle V_0 \rangle_Q$ as a function of IST for off equatorial station Kolhapur. The minimum ΔV is found to be −227 m/s at 22.33 IST, and it is indicated by vertical dash-dotted line.

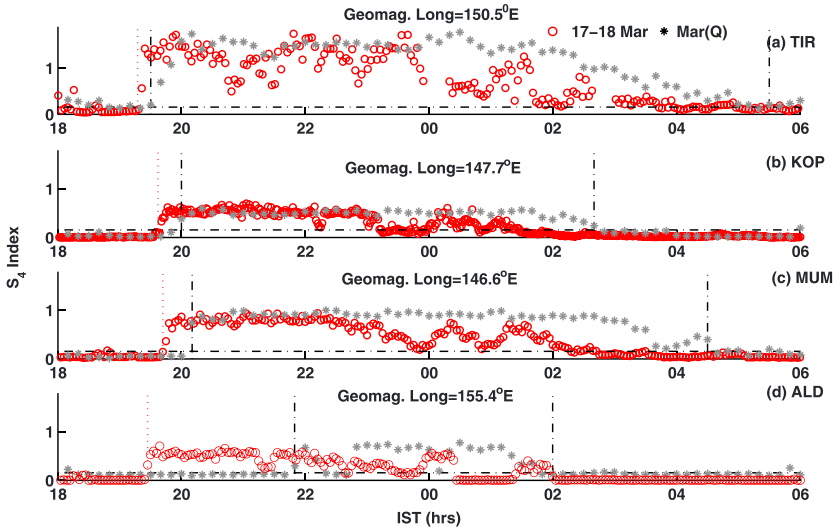

Figure 4. Variation disturbed, 17–18 March (red), time S_4 at (a) Tirunelveli, (b) Kolhapur, (c) Mumbai, and (d) Allahabad is shown as a function of IST. Monthly quiet time variation of peak S_4 for March 2015 is depicted in black in respective subfigures. The geomagnetic longitudes are mentioned for each station in respective subplots.

As discussed in section 2, irregularity drift derived from scintillation data has contribution from both zonal and vertical drifts of irregularity. The perturbation electric field associated with RT plasma instability is considerably eroded nearly 2 h after their initiation [*Bhattacharyya et al.*, 1989, 2001]. Thus, after around 22 LT, estimated $V_0 \approx V_X$ as the contribution of vertical drifts V_Z to estimated V_0 is significantly low. During this phase the irregularities simply drift with the background plasma [*Retterer*, 1999; *Basu et al.*, 1996; *Valladares et al.*, 1996] and hence the estimated V_0 represents the zonal background plasma drift, $U = -E_Z \times B/B^2$, where B is the horizontal component of the geomagnetic field at the station. For 17 March, it is noted that ESF irregularities were evolving ($C_I(x_0, t_m) \leq 0.7$) during the time when large deviation in V_0 is registered. It indicates that the perturbation electric field associated with RT plasma instability is not decayed completely during that time. In such a situation, the perturbation electric field can contribute to the computed V_0 apart from magnetically disturbed time ambient zonal plasma drift U_D. Thus, the observed large deviation in irregularity zonal drift observed at KOP is attributed to U_D and partly to the perturbation electric field linked with RT plasma instability.

Engavale et al. [2006] used spaced receiver scintillations from the same equatorial location, TIR, and examined the effect of geomagnetic storm on zonal plasma drift during 1995–2005. Their study suggests a maximum deviation of 35–120 m/s in zonal plasma drift, which is attributed to magnetically disturbed time-modulated neutral wind pattern. On one occasion, 24 November 2001, the maximum deviation, $|\Delta V_{min}|$, is observed to be ~207 m/s, where it had additional contribution from perturbation electric field. Nevertheless, *Basu et al.* [2010] have reported a westward zonal irregularity drift ~200–300 m/s from Ancon, Peru, which is considerably higher compared to westward zonal irregularity drift of ~100 m/s observed at KOP on 17 March.

3.2. Structuring of ESF Irregularities

Variation of S_4 (red) on 17–18 March is depicted as a function of IST for (a) TIR, (b) KOP, (c) MUM, and (d) ALD in Figure 4. The peak S_4 observed at these stations on quiet days of March 2015 is shown (gray) in respective figures. Vertical black dash-dotted line indicates the average start and end time of scintillation activity on quiet days. Whereas red dotted line indicates the initiation of scintillations on geomagnetically disturbed day. It is noticed that scintillations are initiated 0.21, 0.38, 0.47, and 2.37 h earlier at TIR, KOP, MUM, and ALD, respectively, on 17 March. Except for two quiet days (shown by gray, Figure 4d), no scintillations are observed at ALD throughout March 2015. The interesting observation is the presence of weak-moderate scintillations at low midlatitude station ALD just after sunset (19.5 IST) and their persistence till 02 IST.

Early occurrence of scintillation at ALD on 17 March is unlikely if we compare it with the quiet days of that month. We do observe scintillations at ALD, which are linked with irregularities generated through midlatitude instabilities [*Hanson and Johnson*, 1992; *Kelley and Fukao*, 1991; *Miller et al.*, 1997; *Kelley and Makela*, 2001],

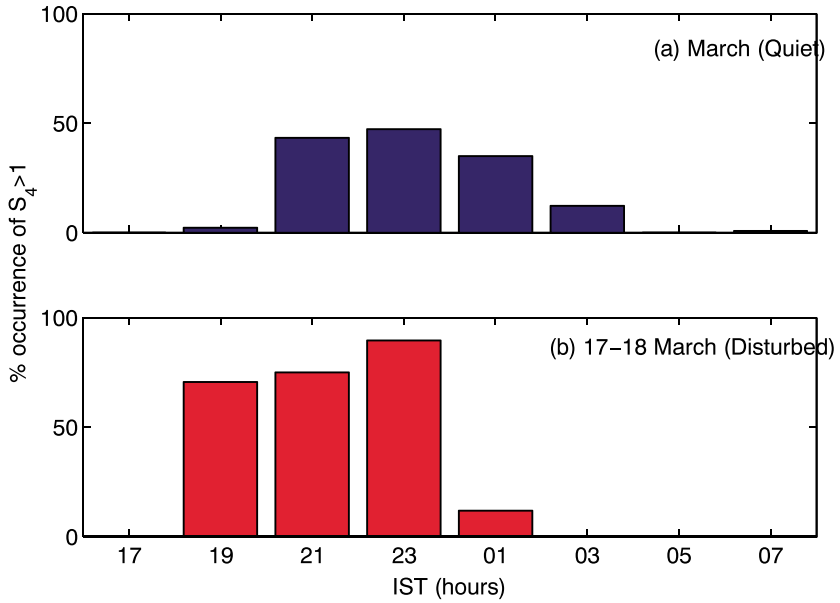

Figure 5. Variation of percentage occurrence of $S_4 > 1$ for (a) quiet days of March and (b) disturbed day, 17–18 March, at Tirunelveli.

and their signatures are manifested in ionograms from that location, as spread *F*. Statistical study using long-term (1990–2003) ionosonde data from an equatorial station in Indian longitude indicates that average peak base height ($h`F_p$) and vertical drift (V_{zp}) of *F* region in the post sunset hours vary from 250 to 500 km and 10 to 40 m/s, respectively, for the $F_{10.7}$ variation of 100–250 [*Kakad et al.*, 2012b]. Geomagnetic storm of 17 March occurred in the descending phase of SC, and the average $F_{10.7}$ is ~ 130. Under such solar flux condition on a quiet day, we expect $h`F_p$ and V_{zp} at the equatorial station TIR in the range of 300–350 km and 20–25 m/s, respectively. Thus, on quiet days of moderate solar activity, the altitudinal extent of intermediate scale ESF irregularities at dip equator may not be adequate to map down to ALD (see Figure 1b). The Canadian Advanced Digital Ionosonde records at Tirunelveli confirm that the base height of *F* region, $h`F$, reached an altitude of more than 560 km in the post sunset hours on 17 March [*Singh et al.*, 2015]. So, on this day ESF irregularities must have reached an altitude $\geq$ 800 km in the post sunset hours so that it could reach ALD through mapping along geomagnetic field lines.

Other important observational feature is the occurrence of strong scintillations $S_4 > 1$ in premidnight hours at TIR. We examined percentage occurrence of $S_4 > 1$ for quiet days of March 2015 and 17–18 March during different time bins. This statistics is shown in Figure 5. It indicates that percentage occurrence of $S_4 > 1$ is higher on 17–18 March as compared to that on quiet days. Strong scintillations are initiated earlier (around 19 h), and it sustained till midnight on 17 March. To investigate this feature in detail, we used theoretical model developed by *Engavale and Bhattacharyya* [2005]. It assumes the layer of irregularity situated at an average height *Z*, and it is divided into n_z number of phase screens separated by free space. In this theoretical model, input parameters like height of irregularity layer, thickness, power spectral index of irregularities, and strength of density perturbations can be varied to obtain the S_4 and $C_l(x_0, t_m)$ in the ground scintillation pattern. We used this model to get the variation of S_4 as a function of irregularity height by varying density perturbations, σ_N, in the range of 7–50%. Theoretical model profiles are shown in Figures 6a and 6b for irregularity power spectral index $m = 5$ and $m = 2$, respectively. It is clear from Figure 6 that shallower power spectral slopes do not produce $S_4 > 1$ for any altitude or irregularity strength. On the other hand, steeper power spectral slopes placed at higher altitudes ($Z > 500$ km) give rise to $S_4 > 1$, when they are associated with strong density perturbations ($\sigma_N = 30\%$). Thus, theoretical model results indicate the presence of large-scale irregularities ($m \geq 5$) with strong density perturbations ($\sigma_N \geq 30\%$) at the raised *F* peak altitude($Z > 500$ km) at dip equatorial station TIR. Also, these conditions must have been sustained in the premidnight hours. Earlier theoretical studies have shown that large-scale irregularities of significant strength tend to focus the incoming radio wave and produce $S_4 > 1$ in the ground scintillation pattern [*Singleton*, 1970; *Booker and MajidiAhi*, 1981].

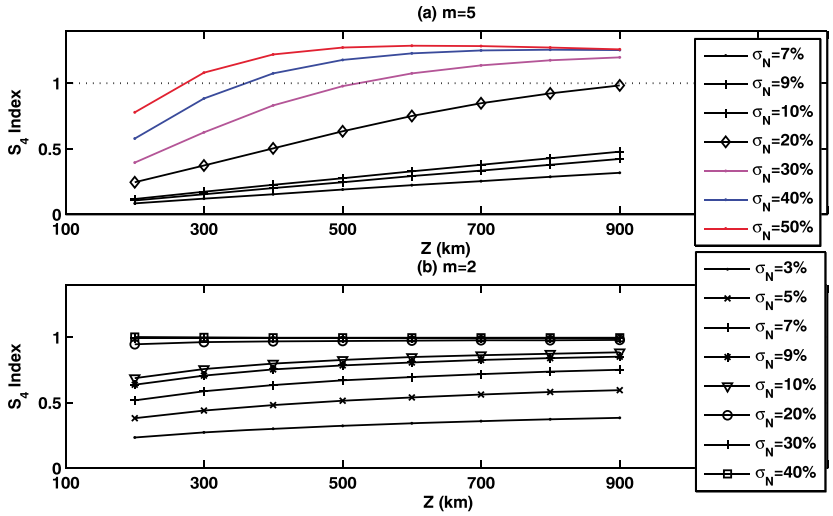

Figure 6. Variation of S_4 as a function of altitude of irregularity layer is obtained theoretically by taking irregularity power spectral index as (a) $m = 5$, (b)$m = 2$, and different density perturbations σ_N.

At the same time above the *F* peak at the equatorial station the irregularity spectrum is shallower as small-scale irregularity develops there before midnight [*Bhattacharyya et al.*, 2014]. These irregularities map down to off equatorial stations. The background *F* region electron density at MUM is higher than that at KOP or ALD as MUM is closer to crest of equatorial ionization anomaly. Hence, S_4 at MUM is higher than that at KOP or ALD. The background electron density at *F* region peak over MUM is higher than that at TIR also, but since the irregularities that map down to the *F* region over MUM have shallower spectrum than that at TIR, S_4 at MUM never exceeds 1.

ESF irregularities are known to follow a power law spectrum $\Phi_N(k) \propto k^{-p}$, where p is three-dimensional power spectral index of irregularity, and it is valid between some inner (r_0) and outer (R_0) scales [*Yeh and Liu*, 1982]. In order to get information on power spectral characteristics of ESF irregularities, we carried out power spectral analysis of weak scintillation events ($0.15 \leq S_4 \leq 0.5$) observed at TIR. The magnitude of slope of the power spectrum on log-log scale gives two-dimensional power spectral index m of ESF irregularities, where $p = m + 1$. This technique fails for the strong scintillations as spatial scales in irregularities and in the ground scintillation pattern do not have one-to-one relationship due to focusing effects. The estimated power spectral indices m are shown as a function of IST for disturbed day, 17–18 March and quiet days of March 2015, in Figure 7. Considerably smaller power spectral indices ($m < 3$) are seen on magnetically disturbed day in the post midnight hours, which is not commonly observed on the quiet days. The power spectral index gives information about the spatial scales of irregularities. The lower (higher) values of m indicate the presence of small (large)-scale length irregularities. It suggests that small-scale ESF irregularities, which as noted earlier, were present at higher altitudes on the disturbed day descended to lower altitudes at a later time.

TIR and ALD scintillation observations, in light of theoretical model result, clearly indicate that ESF irregularities were present at unusually high altitude over Indian region in the post sunset hours on 17 March. It may be noted that the DMSP satellites orbiting at an altitude of 840 km find an EPB occurrence rate of less than 20% in the Indian region during the month of March in the years 1989–2002 [*Burke et al.*, 2004]. Further, *Huang et al.* [2002] have reported that the probability of DMSP satellites detecting an EPB in the Indian sector (82.5°E longitude) in a year has linear dependence on the yearly averaged $F_{10.7}$. The percentage of EPB encounter is given by $0.14\langle F_{10.7}\rangle - 11.2$. Hence, the presence of EPBs at an altitude $\geq$ 800 km in the Indian dip equatorial region during moderate solar flux condition is not a frequent phenomenon. This is attributed to ambient eastward electric field that is responsible for uplift of *F* region in the post sunset hours, which is weaker during lower solar activity. Also, the geomagnetic field in the Indian region is almost twice as strong as that in south Atlantic anomaly region, where the occurrence of EPBs at DMSP height is much more frequent. It is known that through nonlinear evolution of RT plasma instability EPBs rise, evolve, and emerge into topside ionosphere above the dip equator. The presence of small-scale irregularities (~100 m) is more likely at higher altitudes [*Shume and Hysell*, 2004; *Rodrigues et al.*, 2009; *Bhattacharyya et al.*, 2014].

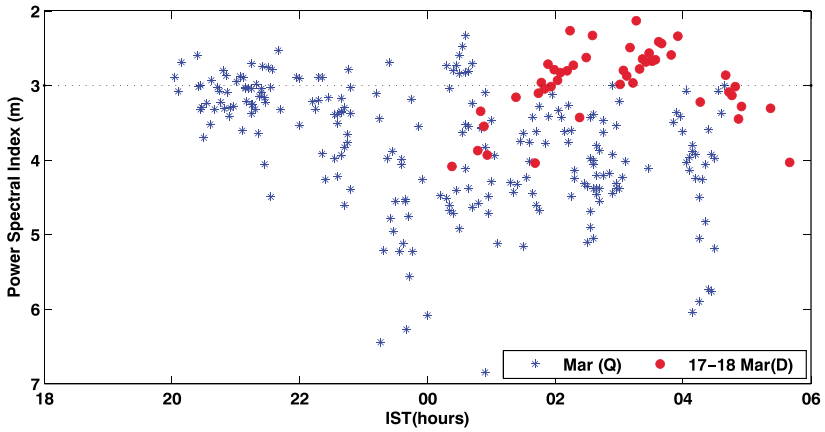

Figure 7. Quiet (black) and disturbed, 17–18 March (red), time variation of power spectral index *m* observed at dip equatorial station Tirunelveli.

4. Geomagnetic Activity and Associated Electric Fields

In order to examine the characteristics of the geomagnetic storm that occurred on that day and the energy inputs at high latitude, we examined the interplanetary parameters and geomagnetic activity indices. Variations of IMF B_Z, interplanetary electric field (IEF) E_y, *Dst*, *AE*, and *ap* on 17 March, as a function of IST, are shown in Figures 8a–8e, respectively. Interplanetary parameters are obtained from http://omniweb.gsfc.nasa.gov/, and the propagation delay from satellite to magnetopause has been taken into account while plotting B_Z and E_y. During this geomagnetic storm, two southward turnings of significant strength, $B_Z \approx -18$ nT and -23 nT, occurred at $t_1 = 11.4$ IST and $t_2 = 17.9$ IST, respectively. These two southward turnings are marked by red and blue dotted rectangles in Figure 8. The time t_e, when maximum effect is seen in zonal plasma drifts at Kolhapur, is marked by vertical dotted line (magenta) in Figure 8. The maximum eastward electric field, rate of change of *AE*, and variation of *ap* associated with first and second southward turnings are given in Table 1. It should be noted that the rate of change of *AE* at second southward turning is nearly 2.6 times that of its rate at first southward turning. Here we also computed the Joule energy deposited at high latitudes using empirical

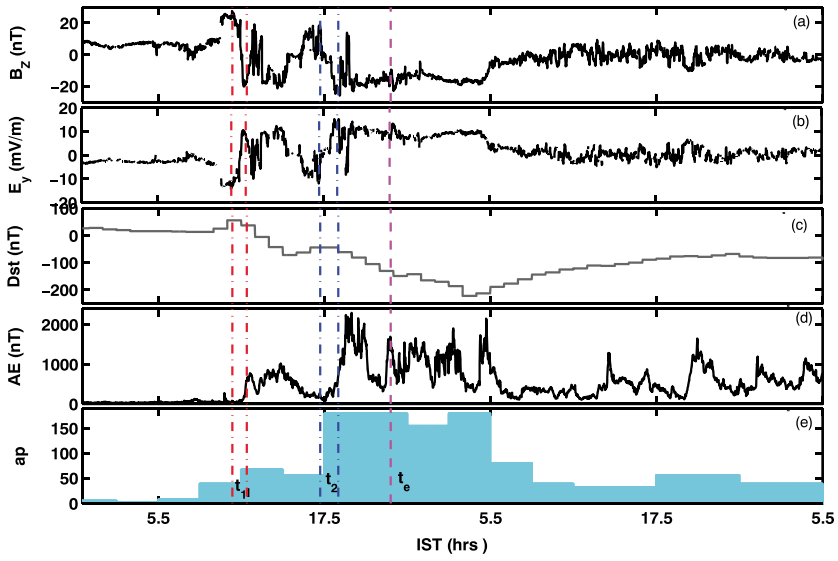

Figure 8. Variation of interplanetary parameters (a) B_Z and (b) E_y and geomagnetic activity indices (c) $SYM - H$, (d) *AE*, and (e) *ap* on 17–18 March 2015 is depicted as a function of IST. Vertical dash-dotted line represents the time of first and second southward turnings represented by t_1 and t_2, respectively. The maximum deviation in zonal plasma drift on 17–18 March at Kolhapur is marked by vertical dotted line (red) at time t_e.

Table 1. List of Various Parameters Considered to Characterize the Geomagnetic Storm

	First Southward Turning	Second Southward Turning
Time	t_1 = 10.85 to 11.89 IST	t_2 = 17.2 to 18.5 IST
Bz_{min}	−18 nT	−23 nT
Ey_{max}	10 mV/m	15 mV/m
d(*AE*)/d*t*	1000 nT/h	2600 nT/h
ap	40–70	155–180
ΔT	$\Delta T_1 = t_2 - t_1$ = 6.35 h	$\Delta T_1 = t_e - t_2$ = 5.1 h
$E_{Joule,\Delta T}$	4.15×10^{15} J	6.88×10^{15} J

relation given by *Akasofu* [1981]. This Joule energy is obtained from time integration of the power given by equation (1)

$$P_{Joule,Akasofu} = 2 * (2 * AE * 10^8)W \quad (1)$$

A factor of 2 accounts for the energy from both hemispheres. Joule energy input at high latitudes is responsible for the development of DD. Thus, we estimated the Joule energy inputs for two phases: (i) from first southward turning t_1 to second southward turning t_2 and (ii) from second southward turning to time t_e of maximum effect in the *F* region. The integration of power (given by equation (1)) from t_1 to t_2 and t_2 to t_e yields the Joule energies of 4.15×10^{15} J and 6.88×10^{15} J during phases 1 and 2, respectively. Although duration of phase 1 (ΔT_1 = 6.35 h) and phase 2 (ΔT_2 = 5.1 h) is nearly the same, the Joule energy deposits at high latitudes increase by 1.7 times for the second phase.

In general, we know that PP electric fields associated with southward turning of IMF B_Z at magnetopause are eastward (westward) during daytime (nighttime). The PP electric field can also be associated with high-latitude substorm activity. During rapidly changing polar cap potential or high-latitude indices like *AE* or *AL*, the high-latitude electric field can leak to low latitudes [*Kikuchi et al.*, 1996, 2000]. *Manoj et al.* [2008] have shown that time delay between IEF and PPEF is less than 5 min at all periods. Also, the IEF can continuously penetrate to the low-latitude ionosphere without significant attenuation for many hours during the main phase of geomagnetic storms [*Huang et al.*, 2005]. But the prompt penetration close to dusk and dawn hours and its variability are not well understood. *Tulasi et al.* [2008] reported that eastward PPEF and associated ESF are likely in all longitudinal sectors where the local time corresponds to post sunset hours during the entire period of the main phase of the storm.

In order to examine the PP electric field on 17 March, we used the real-time ionospheric prompt penetration model, which is available at http://geomag.org/models/PPEFM/RealtimeEF.html. The estimates of disturbed time PPEF and quiet time electric field are obtained for longitude 77°E and 82°E. These electric field profiles are shown in Figure 9. If we consider the contribution of PPEF (~0.6 mV/m), which is eastward and adds positively to the prereversal enhancement (PRE) (~0.7 mV/m), we get net peak eastward electric field of 1.3 mV/m. It corresponds to vertical drift of the order of $V_z = E \times B/B^2$ = 40 m/s, (*B* is taken as 35,000 nT at 300 km altitude). In a recent paper *Singh et al.* [2015] have studied the same geomagnetic storm and reported the presence of vertical drift of 70 m/s, which is higher than the estimates obtained from ionospheric models. So large upliftment of *F* layer on 17 March cannot be simply attributed to PPEF and PRE only.

It may be noted that PPEF occurred in the presence of advancing disturbance dynamo (DD) initiated by former southward turning. The direction and strength of DDEF are determined by many factors like solar flux, season, and local time [*Huang*, 2013]. In general, DDEF is westward in the dayside and close to dusk sector, and it reverses from west to east close to local midnight [*Huang et al.*, 2005; *Li et al.*, 2012]. So the DDEF may not have contributed positively to the PPEF. However, conductivity and neutral wind changes in the middle and low latitudes were already in progress due to first southward turning (10.85–11.89 IST). We speculate that the neutral wind and conductivity changes might have provided appropriate background preconditioning in such a way that it resulted substantially enhanced PPEF. Such possibility is discussed by *Maruyama et al.* [2005].

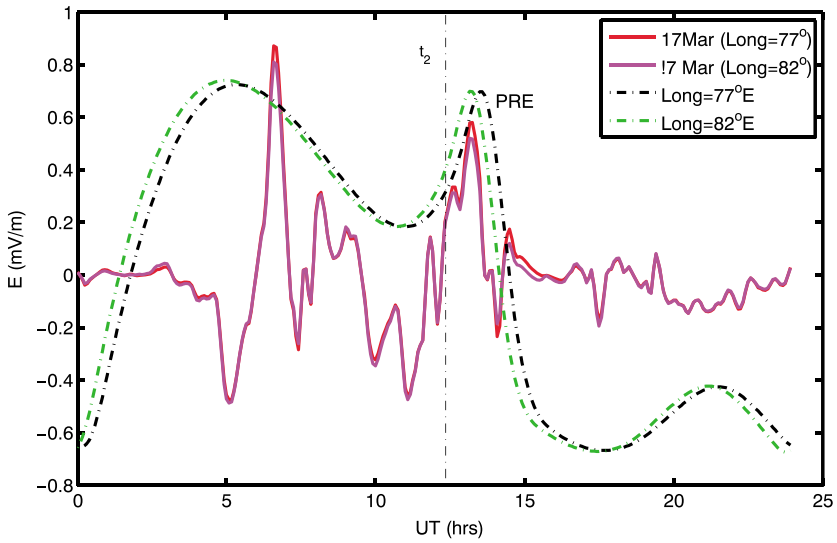

Figure 9. Prompt penetration electric field (PPEF) on 17 March 2015 and quiet time electric field variation obtained from real-time model of the Ionospheric electric fields (http://geomag.org/models/PPEFM/RealtimeEF.html) over magnetic equator at longitude 77° and 82° are shown as a function of UT (IST + 5.5 h). PPEF coincides with the time of PRE. The vertical dash-dotted line indicates the time of second southward turning, t_2.

5. Summary and Conclusions

We have studied the structuring of ESF irregularities produced due to recent intense geomagnetic storm of 17 March 2015. For this purpose we used the spaced receiver amplitude scintillations on 251 MHz from a network of stations in Indian longitude. Some of the peculiar observations on 17 March are discussed with emphasis on the structuring of the developed EPBs and associated ESF irregularities. The present study yields the following results: (i) Geomagnetic activity on 17 March triggered EPBs that rise to unusually higher altitudes resulting in wider latitudinal extent over Indian longitude in the post sunset hours, and (ii) the large-scale structures with strong density perturbations (30%) are likely to be present at raised equatorial *F* peak with smaller-scale length irregularities at even higher altitudes. Theoretical model results are consistent with the observations. It confirms that large-scale (~1 km) ESF structures resulting in irregularity spectrum with a steep slope over the scale range 100 m – 1 km, present at equatorial *F* peak on 17 March, produced strong scintillations ($S_4 \geq 1$) on VHF radio wave signal. This strong focusing effect persisted throughout premidnight hours. Shorter-scale (few hundreds of meters) irregularities were present above the equatorial *F* peak that mapped down to higher latitudes producing a shallower irregularity spectrum there. The real-time ionospheric electric field model confirms the generation of large eastward PPEF in the equatorial *F* region at the time of prereversal enhancement (PRE) in Indian longitude. However, the model estimate is relatively smaller compared to the observed vertical drift of 70 m/s. Thus, large upliftment of *F* layer on 17 March cannot be simply assigned to PPEF and PRE. We speculate that the neutral wind and conductivity changes driven by earlier magnetic activity might have offered the appropriate background preconditioning so that it enhanced the PPEF effect associated with the second southward turning of IMF B_z. The other important observational feature is the large deviation of 230 m/s in zonal irregularity drift at off equatorial station KOP, which is larger compared to earlier reports from the same station. It is attributed to disturbed time zonal wind and perturbation electric field linked with RT instability. The perturbation electric field associated with instability has both vertical and zonal components [*Retterer*, 2010], out of which the vertical component contributes to zonal irregularity drift.

Acknowledgments
We thank the CIRES team for real-time PPEEFM model at http://geomag.org/models/PPEFM/RealtimeEF.html. We thank the Omniweb group for interplanetary parameters and geomagnetic activity indices available at http://omniweb.gsfc.nasa.gov/. Thanks are due to K.U. Nair, Ananthi, Rupesh, P. Tiwari, and S. Banola for their technical support on scintillation experiment. A.B. acknowledges the Science and Engineering Research Board for a J.C. Bose national fellowship.

References

Abdu, M. A., J. H. Sastri, J. MacDougall, I. S. Batista, and J. H. A. Sobral (1997), Equatorial disturbance dynamo electric field longitudinal structures and spread *F*: A case study from GUARA/EITS compaigns, *Geophys. Res. Lett.*, *24*(13), 1707 – 1710.

Abdu, M. A. (2012), Equatorial spread F/plasma bubble irregularities under storm time disturbance electric fields, *J. Atmos. Terr. Phys.*, *75*, 44 – 56, doi:10.1016/j.jastp.2011.04.024.

Akasofu, S. I. (1981), Energy coupling between the solar wind and the magnetosphere, *Space Sci. Rev.*, *28*, 121 – 190.

Basu, S., et al. (1996), Scintillations, plasma drifts, and neutral winds in the equatorial ionosphere after sunset, *J. Geophys. Res.*, *101*(A12), 26,795 – 26,809.

Basu, S., S. Basu, E. MacKenzie, C. Bridgwood, C. E. Valladares, K. M. Groves, and C. Carrano (2010), Specification of the occurrence of equatorial ionospheric scintillations during the main phase of large magnetic storms within solar cycle 23, *Radio Sci.*, *45*, RS5009, doi:10.1029/2009RS004343.

Bhattacharyya, A., S. J. Franke, and K. C. Yeh (1989), Characteristic velocity of equatorial *F* region irregularities determined from spaced receiver scintillation data, *J. Geophys. Res.*, *94*(A9), 11,959–11,969.

Bhattacharyya, A., S. Basu, K. M. Groves, C. E. Valladares, and R. Sheehan (2001), Dynamics of equatorial *F* region irregularities from spaced receiver scintillation observations, *Geophys. Res. Lett.*, *28*(1), 119–122.

Bhattacharyya, A., K. M. Groves, S. Basu, H. Kuenzler, C. E. Valladares, and R. Sheehan (2003), L-band scintillation activity and space-time structure of low-latitude UHF scintillations, *Radio Sci.*, *38*(1), 1004, doi:10.1029/2002RS002711.

Bhattacharyya, A., B. Kakad, S. Sripathi, K. Jeeva, and K. U. Nair (2014), Development of intermediate scale structure near the peak of the *F* region within an equatorial plasma bubble, *J. Geophys. Res. Space Physics*, *119*, 3066–3076, doi:10.1002/2013JA019619.

Blanc, M., and A. D. Richmond (1980), The ionospheric disturbance dynamo, *J. Geophys. Res.*, *85*, 1669–1686.

Briggs, B. H. (1984), The analysis of spaced sensor records by correlation techniques, in *Middle Atmosphere Program, Handbook for MAP*, vol. 13, edited by R. A. Vincent, pp. 166–186, Int. Counc. of Sci. Unions, Paris.

Booker, H. G., and G. MajidiAhi (1981), Theory of refractive scattering in scintillation phenomena, *J. Atmos. Terr. Phys.*, *43*, 1199–1214.

Burke, W. J., L. C. Gentile, C. Y. Huang, C. E. Valladares, and S. Y. Su (2004), Longitudinal variability of equatorial plasma bubbles observed by DMSP and ROCSAT 1, *J. Geophys. Res.*, *109*, A12301, doi:10.1029/2004JA010583.

Engavale, B., and A. Bhattacharyya (2005), Spatial correlation function of intensity variations in the ground scintillation pattern produced by equatorial spread F irregularities, *Indian J. Radio Space Phys.*, *34*, 23–32.

Engavale, B., K. Jeeva, K. U. Nair, and A. Bhattacharyya (2005), Solar flux dependence of coherence scales in scintillation patterns produced by ESF irregularities, *Ann. Geophys.*, *23*, 3261–3266.

Engavale, B., K. Jeeva, K. U. Nair, and A. Bhattacharyya (2006), Effect of magnetic activity on equatorial F region plasma drifts, paper presented at ILWS WORKSHOP 2006, p. 432, GOA, 19–24 Feb.

Fejer, B. G., and L. Scherliess (1995), Time dependent response of equatorial ionospheric electric fields to magnetospheric disturbances, *Geophys. Res. Lett.*, *22*, 851–854.

Fejer, B. G., R. W. Spiro, R. A. Wolf, and J. C. Foster (1990), Latitudinal variation of perturbation electric fields during magnetically disturbed periods: 1986 SUNDIAL observations and model results, *Ann. Geophys.*, *8*, 441–454.

Fejer, B. G., E. R. dePaula, S. A. González, and R. F. Woodman (1991), Average vertical and zonal F region plasma drifts over Jicamarca, *J. Geophys. Res.*, *96*(A8), 13,901–13,906, doi:10.1029/91JA01171.

Hanson, W. B., and F. S. Johnson (1992), Lower midlatitude ionospheric disturbances and the Perkins instability, *Planet. Space Sci.*, *12*, 1615–1630.

Huang, C. M. (2013), Disturbance dynamo electric fields in response to geomagnetic storms occurring at different universal times, *J. Geophys. Res. Space Physics*, *118*, 496–501, doi:10.1029/2012JA018118.

Huang, C. S., J. C. Foster, and M. C. Kelley (2005), Long-duration penetration of the interplanetary electric field to the low-latitude ionosphere during the main phase of magnetic storms, *J. Geophys. Res.*, *110*, A11309, doi:10.1029/2005JA011202.

Huang, C. Y., W. J. Burke, J. S. Machuzak, L. C. Gentile, and P. J. Sultan (2002), Equatorial plasma bubbles observed by DMSP satellites during a full solar cycle: Toward a global climatology, *J. Geophys. Res.*, *107*(A12), 1434, doi:10.1029/2002JA009452.

Kakad, B., K. Jeeva, K. U. Nair, and A. Bhattacharyya (2007), Magnetic activity linked generation of nighttime equatorial spread *F* irregularities, *J. Geophys. Res.*, *112*, A07311, doi:10.1029/2006JA012021.

Kakad, B., D. Tiwari, and T. K. Pant (2011), Study of disturbance dynamo effects at nighttime equatorial F region in Indian longitude, *J. Geophys. Res.*, *116*, A12318, doi:10.1029/2011JA016626.

Kakad, B., C. K. Nayak, and A. Bhattacharyya (2012a), Power spectral characteristics of ESF irregularities during magnetically quiet and disturbed days, *J. Atmos. Sol. Terr. Phys.*, *81*, 41–49, doi:10.1016/j.jastp.2012.04.008.

Kakad, B., D. Tiwari, and T. K. Pant (2012b), Study of post sunset vertical plasma drift at equatorial F-region using long-term (1990–2003) ionosonde measurements in Indian longitude, *J. Atmos. Sol. Terr. Phys.*, *80*, 239–246, doi:10.1016/j.jastp.2012.02.004.

Kelley, M. C., and S. Fukao (1991), Turbulent upwelling of the midlatitude ionosphere: 2. Theoretical framework, *J. Geophys. Res.*, *96*, 3747–3753.

Kelley, M. C., and J. J. Makela (2001), Resolution of the discrepancy between experiment and theory of midlatitude *F*-region structures, *Geophys. Res. Lett.*, *28*, 2589–2592.

Keskinen, M. J., S. L. Ossakow, B. G. Fejer, and J. Emmert (2006), Evolution of equatorial ionospheric bubbles during a large auroral electrojet index increase in the recovery phase of a magnetic storm, *J. Geophys. Res.*, *111*, A02303, doi:10.1029/2005JA011352.

Kikuchi, T., H. Lühr, T. Kitamura, O. Saka, and K. Schlegel (1996), Direct penetration of the polar electric field to the equator during a DP 2 event as detected by the auroral and equatorial magnetometer chains and the EISCAT radar, *J. Geophys. Res.*, *101*(A8), 17,161–17,173.

Kikuchi, T., H. Luhr, K. Schlegel, H. Tachihara, M. Shinohara, and T. L. Kitamura (2000), Penetration of auroral electric fields to the equator during a substorm, *J. Geophys. Res.*, *105*, 23,251–23,261.

Li, G., et al. (2010), Longitudinal development of low latitude ionospheric irregularities during the geomagnetic storms of July 2004, *J. Geophys. Res.*, *115*, A04304, doi:10.1029/2009JA014830.

Li, J., G. Ma, T. Maruyama, and Z. Li (2012), Mid-latitude ionospheric irregularities persisting into late morning during the magnetic storm on 19 March 2001, *J. Geophys. Res.*, *117*, A08304, doi:10.1029/2012JA017626.

Ma, G., and T. Maruyama (2006), A super bubble detected by dense GPS network at east Asian longitudes, *Geophys. Res. Lett.*, *33*, L21103, doi:10.1029/2006GL027512.

Manoj, C., S. Maus, H. Luhr, and P. Alken (2008), Penetration characteristics of the interplanetary electric field to the daytime equatorial ionosphere, *J. Geophys. Res.*, *113*, A12310, doi:10.1029/2008JA013381.

Martinis, C. R., M. J. Mendillo, and J. Aarons (2005), Toward a synthesis of equatorial spread *F* onset and suppression during geomagnetic storms, *J. Geophys. Res.*, *110*, A07306, doi:10.1029/2003JA010362.

Maruyama, N., A. D. Richmond, T. J. Fuller-Rowell, M. V. Codrescu, S. Sazykin, F. R. Toffoletto, R. W. Spiro, and G. H. Millward (2005), Interaction between direct penetration and disturbance dynamo electric fields in the storm-time equatorial ionosphere, *Geophys. Res. Lett.*, *32*, L17105, doi:10.1029/2005GL023763.

Miller, C. A., W. E. Swartz, M. C. Kelley, M. Mendillo, D. Nottingham, J. Scali, and B. Reinisch (1997), Electrodynamics of midlatitude spread *F*: 1. Observations of unstable, gravity wave-induced ionospheric electric fields at tropical latitudes, *J. Geophys. Res.*, *102*, 11,521–11,532.

Nishioka, M., A. Saito, and T. Tsugawa (2008), Occurrence characteristics of plasma bubble derived from global ground-based GPS receiver networks, *J. Geophys. Res.*, *113*, A05301, doi:10.1029/2007JA012605.

Singh, R., S. Sripathi, S. Sreekumar, S. Banola, K. Emperumal, P. Tiwari, and B. S. Kumar (2015), Low-latitude ionosphere response to super geomagnetic storm of 17/18 March 2015: Results from a chain of ground-based observations over Indian sector, *J. Geophys. Res. Space Physics*, *120*, 10,864–10,882, doi:10.1002/2015JA021509.

Retterer, J. M. (1999), Theoretical model for fast equatorial bubbles, paper presented at 1999 Ionospheric Effects Symposium, p. 688, Alexandria, Virginia.

Retterer, J. M. (2010), Forecasting low-latitude radio scintillation with 3-D ionospheric plume models: 1. Plume model, *J. Geophys. Res.*, *115*, A03306, doi:10.1029/2008JA013839.

Rodrigues, F. S., M. C. Kelley, P. A. Roddy, D. E. Hunton, R. F. Pfaff, O. de La Beaujardière, and G. S. Bust (2009), C/NOFS observations of intermediate and transitional scale-size equatorial spread *F* irregularities, *Geophys. Res. Lett.*, *36*, L00C05, doi:10.1029/2009GL038905.

Sastri, J. H. (1999), Post-midnight onset of spread-F at Kodaikanal during the June solstice of solar minimum, *Ann. Geophys.*, *17*, 1111–1115.

Scherliess, L., and B. G. Fejer (1997), Storm time dependence of equatorial disturbance dynamo zonal electric fields, *J. Geophys. Res.*, *102*, 24,037–24,046.

Singleton, D. G. (1970), Saturation and focusing effects in radio star and satellite scintillation, *J. Atmos. Terr. Phys.*, *32*, 187–208.

Shume, E. B., and D. L. Hysell (2004), Spectral analysis of plasma drift measurements from the AE-E satellite: Evidence of an inertial subrange in equatorial spread F, *J. Atmos. Sol. Terr. Phys.*, *66*, 57–65.

Spiro, R. W., R. A. Wolf, and B. G. Fejer (1988), Penetrating of high-latitude-electric-field effects to low latitudes during SUNDIAL 1984, *Ann. Geophys.*, *6*, 39–49.

Sutton, E. K., J. M. Forbes, and R. S. Nerem (2005), Global thermospheric neutral density and wind response to the severe 2003 geomagnetic storms from CHAMP accelerometer data, *J. Geophys. Res.*, *110*, A09S40, doi:10.1029/2004JA010985.

Tulasi Ram, S., P. V. S. Rama Rao, D. S. V. V. D. Prasad, K. Niranjan, S. Gopi Krishna, R. Sridharan, and S. Ravindran (2008), Local time dependent response of postsunset ESF during geomagnetic storms, *J. Geophys. Res.*, *113*, A07310, doi:10.1029/2007JA012922.

Valladares, C. E., R. Sheehan, S. Basu, H. Kuenzler, and J. Espinoza (1996), The multi-instrumented studies of equatorial thermosphere aeronomy scintillation system: Climatology of zonal drifts, *J. Geophys. Res.*, *101*(A12), 26,839–26,850.

Yadav, V., B. Kakad, T. K. Pant, A. Bhattacharyya, and D. S. V. V. D. Prasad (2015), Study of equatorial *E* region irregularities using rare daytime VHF scintillation observations, *J. Geophys. Res. Space Physics*, *120*, 9074–9086, doi:10.1002/2015JA021320.

Yeh, K. C., and C. H. Liu (1982), Radio wave scintillations in the ionosphere, *Proc. IEEE*, *70*, 324–360.